Chapter 6

Conclusions

This thesis has presented a hybrid full-field experimental method combining phase-shifting photoelasticity and transmission Coherent Gradient Sensing for in-plane tensorial stress determination for fracture studies. In order for this method to achieve its goals, a new analysis for transmission wavefront shearing interferometry applied to photoelastic materials has been developed and experimentally verified for the specific wavefront shearing interferometer Coherent Gradient Sensing. The hybrid experimental method has been developed and experimentally verified for photoelastic materials by good comparison between experimental and theoretical stress fields for a compressed polycarbonate plate with a side V-notch. The hybrid experimental method has also been validated for full-field tensorial stress determination around Mode I–dominant cracks in photoelastic materials, a study that is the first to achieve these goals, serving as the foundation for future research in extending this method for fracture studies in anisotropic materials.

The new analysis of transmission wavefront shearing interferometry for photoelastic materials derives an intensity expression I^{image} for the complicated interference pattern that, in general, is the sum of two interference patterns such that $I^{image} = I_o + I_{1o}\cos[\varphi_{sum} + \varphi_{diff}] + I_{2o}\cos[\varphi_{sum} - \varphi_{diff}]$ (Equation (2.16)); φ_{sum} is the phase related to $\sigma_1 + \sigma_2$ and is the only phase that results for these interferometers applied to optically isotropic materials, φ_{diff} is a phase related to $\sigma_1 - \sigma_2$, and I_{1o} and I_{2o} are coefficients determined by the polarization of the input electric field. The control of the input electric field polarization by polarization optics prior to the photoelastic specimen, in addition to phase-shifting techniques, allow for determination of the desired φ_{sum}. This analysis

has been verified using a compressed polycarbonate plate with a side V-notch using CGS with the experimental phase maps comparing well with theory based on Williams (1952). This analysis serves as the governing theory for determination of x and y derivatives of $\sigma_1+\sigma_2$ for the hybrid experimental method presented in this thesis.

A six-step phase-shifting photoelasticity method has been presented utilizing different angles for the polarization optics in a circular polariscope to obtain six images related to $\sigma_1 - \sigma_2$ and the isoclinic angle, α, which is the angle between the Cartesian and principal coordinate systems. This method allows for full-field determination of $\sigma_1 - \sigma_2$ and α. Since the first two polarization optics of the circular polariscope, a polarizer and $\lambda/4$ plate set for circular polarization of the electric field prior to the specimen, are also useful for determination of φ_{sum} from CGS, then a non-polarizing beamsplitter or a translating mirror immediately after the sample allows for these two experimental techniques to be combined to investigate the same field of view of a specimen. The phase-shifting techniques produce "wrapped" phase fields that require unwrapping before the stress fields can be determined, a task achieved by a data-quality–guided unwrapping algorithm by Ghiglia and Romero (1994) based on preconditioned conjugate gradient (PCG) numerical methods used to solve discrete Poisson equations. A slightly modified version of the algorithm has been implemented for integration of the x and y derivatives of stress to determine $\sigma_1 + \sigma_2 + c_i$, where the constant of integration c_i is determined by a traction free boundary condition. The in-plane tensorial stress components can then be determined from full-field $\sigma_1 + \sigma_2$, $\sigma_1 - \sigma_2$, and α, as demonstrated for a compressed polycarbonate plate with a side V-notch. Some potential error sources have been identified as rotational misalignment of the polarization optics and transmission and reflectance coefficients of the non-polarizing beamsplitter, and mitigation techniques have been developed to minimize error, particularly in the isoclinic angle. Despite these error sources, the experimental and theoretical data have good agreement. This experimental verification of the hybrid experimental method is the basis for the application of the method for determination of the in-plane tensorial stress around a loaded crack in a photoelastic material.

The first study to experimentally determine full-field in-plane tensorial stress around a crack in a

photoelastic material has been presented. The hybrid method has been applied to Mode I–dominant cracks in Homalite-100 for small fields of view, for a range of Mode I stress intensity factors from around one-quarter to just below the fracture toughness of Homalite-100, and for a small range of mode-mixity K_{II}/K_I from -0.010 to 0.020. The experimental stress fields show K-dominant behavior, allowing for excellent comparison to full-field theoretical data based on the 2D asymptotic crack solution using the experimentally calculated K_I and K_{II} values. These values have been calculated from stress fields incorporating both CGS and photoelasticity data and allow for global error less than 5% for most fields and no greater than 7.8%, showing that the two techniques work well together for stress determination around cracks. Common error sources identified in Chapter 3 are characterized for this application and can be mitigated with careful experimentation and with improved analysis algorithms. This study has successfully met the objective of this thesis: to apply a hybrid experimental method for full-field in-plane tensorial stress determination suitable for fracture studies in photoelastic materials with the ability to view local stresses around a crack for small (mm-scale) fields of view for small specimens. This study is the foundation for future research in extending this method for fracture studies in anisotropic materials.

Future research discussed in this thesis for the hybrid CGS-photoelasticity experimental method involves improvements to the current method and then extension of it for fracture studies in anisotropic materials, particularly crystalline materials. Errors associated with the rotational misalignment of the polarization optics and to the non-polarizing beamsplitter may be mitigated with careful alignment procedures and by characterizing the quality and tolerances of the optics. A robust algorithm should be developed to improve the user-correction of any remaining errors due to these sources in the isoclinic angle data. Since this experimental method ultimately uses the $\sigma_1+\sigma_2$ stress field data, then the derivative assumption relating the CGS phases to spatial derivatives of stresses and the error associated with this assumption may be eliminated by treating the phases as finite differences based on staggered grids. The vertical and horizontal phase data may be used in an algorithm, which requires future implementation, to solve a discrete Poisson equation to determine $\sigma_1+\sigma_2$. Extending the experimental method to crystalline materials requires (i) a detectable photoe-

lastic effect from the crystal and (ii) extensive analysis of the interference patterns in the individual experimental techniques. A preliminary investigation of the ferroelectric $BaTiO_3$ has shown that this crystal has a detectable photoelastic effect, but this effect is confounded by the spontaneous polarization of the ferroelectric. Further analysis is required to determine the physical meaning of interference patterns from both photoelasticity and CGS for this ferroelectric. Established theories such as photoelasticity for crystals and the electro-optic effect serve as tools for new analyses that extend the CGS-photoelasticity experimental method to meet its ultimate goal of full-field stress determination for fracture criteria development for active anisotropic materials.

Appendix A

Stress in Principal, Cartesian, and Polar Coordinate Systems

A.1 Relations Between Stress Fields in Principal, Cartesian, and Polar Coordinate Systems

A.1.1 Principal and Cartesian Coordinate Systems

Transforming the 2D stress tensor $\boldsymbol{\sigma}$ from Cartesian to the principal coordinate system and vice versa requires the rotation matrix $\mathbf{R}_\alpha$, given in Equation (A.1), where α is the angle between the Cartesian and principal coordinate systems, as shown in Figure A.1. Equation (A.2) shows transforming $\boldsymbol{\sigma}$ from Cartesian to principal coordinates. Equation (A.3) shows transforming $\boldsymbol{\sigma}$ from principal to Cartesian coordinates in terms of the sum and differences of the principal stresses.

$$\mathbf{R}_\alpha = \begin{bmatrix} \cos(\alpha) & -\sin(\alpha) \\ \sin(\alpha) & \cos(\alpha) \end{bmatrix} \tag{A.1}$$

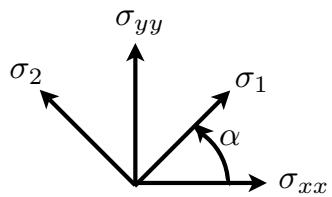

Figure A.1: Schematic of Cartesian and principal coordinate systems

$$
\begin{aligned}
\begin{bmatrix} \sigma_1 & 0 \\ 0 & \sigma_2 \end{bmatrix} &= \mathbf{R}_\alpha^{\mathbf{T}} \begin{bmatrix} \sigma_{xx} & \sigma_{xy} \\ \sigma_{xy} & \sigma_{yy} \end{bmatrix} \mathbf{R}_\alpha \\
&= \mathbf{R}_\alpha^{\mathbf{T}} \begin{bmatrix} \sigma_{xx}\cos(\alpha) + \sigma_{xy}\sin(\alpha) & -\sigma_{xx}\sin(\alpha) + \sigma_{xy}\cos(\alpha) \\ \sigma_{yy}\sin(\alpha) + \sigma_{xy}\cos(\alpha) & \sigma_{yy}\cos(\alpha) - \sigma_{xy}\sin(\alpha) \end{bmatrix} \\
&= \begin{bmatrix} [\sigma_{xx}\cos^2(\alpha) + \sigma_{yy}\sin^2(\alpha) & [(\sigma_{yy} - \sigma_{xx})\cos(\alpha)\sin(\alpha) \\ \quad + 2\sigma_{xy}\cos(\alpha)\sin(\alpha)] & \quad + \sigma_{xy}(\cos^2(\alpha) - \sin^2(\alpha))] \\ [(\sigma_{yy} - \sigma_{xx})\cos(\alpha)\sin(\alpha) & [\sigma_{xx}sin^2(\alpha) + \sigma_{yy}\cos^2(\alpha) \\ \quad + \sigma_{xy}(\cos^2(\alpha) - \sin^2(\alpha))] & \quad - 2\sigma_{xy}\cos(\alpha)\sin(\alpha)] \end{bmatrix} \\
&= \begin{bmatrix} [\sigma_{xx}\left(\frac{1+\cos(2\alpha)}{2}\right) & [(\sigma_{yy} - \sigma_{xx})\left(\frac{\sin(2\alpha)}{2}\right) \\ \quad + \sigma_{yy}\left(\frac{1-\cos(2\alpha)}{2}\right) + \sigma_{xy}\sin(2\alpha)] & \quad + \sigma_{xy}\cos(2\alpha)] \\ [(\sigma_{yy} - \sigma_{xx})\left(\frac{\sin(2\alpha)}{2}\right) & [\sigma_{xx}\left(\frac{1-\cos(2\alpha)}{2}\right) \\ \quad + \sigma_{xy}\cos(2\alpha)] & \quad + \sigma_{yy}\left(\frac{1+\cos(2\alpha)}{2}\right) - \sigma_{xy}\sin(2\alpha)] \end{bmatrix} \\
&= \begin{bmatrix} [\frac{1}{2}(\sigma_{xx} + \sigma_{yy}) + \frac{1}{2}(\sigma_{xx} - \sigma_{yy})\cos(2\alpha) & [-\frac{1}{2}(\sigma_{xx} - \sigma_{yy})\sin(2\alpha) \\ \quad + \sigma_{xy}\sin(2\alpha)] & \quad + \sigma_{xy}\cos(2\alpha)] \\ [-\frac{1}{2}(\sigma_{xx} - \sigma_{yy})\sin(2\alpha) & [\frac{1}{2}(\sigma_{xx} + \sigma_{yy}) - \frac{1}{2}(\sigma_{xx} - \sigma_{yy})\cos(2\alpha) \\ \quad + \sigma_{xy}\cos(2\alpha)] & \quad - \sigma_{xy}\sin(2\alpha)] \end{bmatrix}
\end{aligned}
\tag{A.2}
$$

$$
\begin{aligned}
\begin{bmatrix} \sigma_{xx} & \sigma_{xy} \\ \sigma_{xy} & \sigma_{yy} \end{bmatrix} &= \mathbf{R}_\alpha \begin{bmatrix} \sigma_1 & 0 \\ 0 & \sigma_2 \end{bmatrix} \mathbf{R}_\alpha^{\mathbf{T}} \\
&= \mathbf{R}_\alpha \begin{bmatrix} \sigma_1 \cos(\alpha) & \sigma_1 \sin(\alpha) \\ -\sigma_2 \sin(\alpha) & \sigma_2 \cos(\alpha) \end{bmatrix} \\
&= \begin{bmatrix} \sigma_1 \cos^2(\alpha) + \sigma_2 \sin^2(\alpha) & (\sigma_1 - \sigma_2)\cos(\alpha)\sin(\alpha) \\ (\sigma_1 - \sigma_2)\cos(\alpha)\sin(\alpha) & \sigma_1 \sin^2(\alpha) + \sigma_2 \cos^2(\alpha) \end{bmatrix} \\
&= \begin{bmatrix} \sigma_1\left(\frac{1+\cos(2\alpha)}{2}\right) + \sigma_2\left(\frac{1-\cos(2\alpha)}{2}\right) & (\sigma_1 - \sigma_2)\left(\frac{\sin(2\alpha)}{2}\right) \\ (\sigma_1 - \sigma_2)\left(\frac{\sin(2\alpha)}{2}\right) & \sigma_1\left(\frac{1-\cos(2\alpha)}{2}\right) + \sigma_2\left(\frac{1+\cos(2\alpha)}{2}\right) \end{bmatrix} \\
&= \begin{bmatrix} \frac{1}{2}(\sigma_1 + \sigma_2) + \frac{1}{2}(\sigma_1 - \sigma_2)\cos(2\alpha) & \frac{1}{2}(\sigma_1 - \sigma_2)\sin(2\alpha) \\ \frac{1}{2}(\sigma_1 - \sigma_2)\sin(2\alpha) & \frac{1}{2}(\sigma_1 + \sigma_2) - \frac{1}{2}(\sigma_1 - \sigma_2)\cos(2\alpha) \end{bmatrix}
\end{aligned}
\tag{A.3}
$$

A.1.2 Polar and Cartesian Coordinate Systems

Transforming the 2D stress tensor $\boldsymbol{\sigma}$ from Cartesian to the polar coordinate system and vice versa requires the rotation matrix $\mathbf{R}_\theta$, given in Equation (A.4), where θ is the angle between the Cartesian x-axis and the radius vector. Equation (A.5) shows transforming $\boldsymbol{\sigma}$ from Cartesian to polar coordinates. Equation (A.6) shows transforming $\boldsymbol{\sigma}$ from polar to Cartesian coordinates. Since the simplifications are similar to the equations in Section (A.1.1), not all the steps are shown.

$$
\mathbf{R}_\theta = \begin{bmatrix} \cos(\theta) & -\sin(\theta) \\ \sin(\theta) & \cos(\theta) \end{bmatrix} \tag{A.4}
$$

$$\begin{bmatrix} \sigma_{rr} & \sigma_{r\theta} \\ \sigma_{r\theta} & \sigma_{\theta\theta} \end{bmatrix} = \mathbf{R}_\theta^{\mathbf{T}} \begin{bmatrix} \sigma_{xx} & \sigma_{xy} \\ \sigma_{xy} & \sigma_{yy} \end{bmatrix} \mathbf{R}_\theta$$

$$= \begin{bmatrix} [\sigma_{xx}\cos^2(\theta) + \sigma_{yy}\sin^2(\theta) & [-\frac{1}{2}(\sigma_{xx} - \sigma_{yy})\sin(2\theta) \\ \quad +\sigma_{xy}\sin(2\theta)] & \quad +\sigma_{xy}\cos(2\theta)] \\ [-\frac{1}{2}(\sigma_{xx} - \sigma_{yy})\sin(2\theta) & [\sigma_{xx}\sin^2(\theta) + \sigma_{yy}\cos^2(\theta) \\ \quad +\sigma_{xy}\cos(2\theta)] & \quad -\sigma_{xy}\sin(2\theta)] \end{bmatrix} \tag{A.5}$$

$$\begin{bmatrix} \sigma_{xx} & \sigma_{xy} \\ \sigma_{xy} & \sigma_{yy} \end{bmatrix} = \mathbf{R}_\theta \begin{bmatrix} \sigma_{rr} & \sigma_{r\theta} \\ \sigma_{r\theta} & \sigma_{\theta\theta} \end{bmatrix} \mathbf{R}_\theta^{\mathbf{T}}$$

$$= \begin{bmatrix} [\sigma_{rr}\cos^2(\theta) + \sigma_{\theta\theta}\sin^2(\theta) & [\frac{1}{2}(\sigma_{rr} - \sigma_{\theta\theta})\sin(2\theta) \\ \quad -\sigma_{r\theta}\sin(2\theta)] & \quad +\sigma_{r\theta}\cos(2\theta)] \\ [\frac{1}{2}(\sigma_{rr} - \sigma_{\theta\theta})\sin(2\theta) & [\sigma_{rr}\sin^2(\theta) + \sigma_{\theta\theta}\cos^2(\theta) \\ \quad +\sigma_{r\theta}\cos(2\theta)] & \quad +\sigma_{r\theta}\sin(2\theta)] \end{bmatrix} \tag{A.6}$$

A.1.3 Polar and Principal Coordinate Systems

The 2D stress tensor $\boldsymbol{\sigma}$ may be transformed from Cartesian to the Polar coordinate system and vice versa using the relations in Sections A.1.1–A.1.2. The stress components σ_{rr}, $\sigma_{r\theta}$, and $\sigma_{\theta\theta}$ are given in terms of the principal stresses, the principal direction (in terms of the angle α), and the angle θ, as given in Equations (A.7)–(A.9). The principal stress components are given in terms of the σ_{rr}, $\sigma_{r\theta}$, and $\sigma_{\theta\theta}$, the principal direction, and the angle θ, as given in Equation (A.10).

$$\begin{aligned}
\sigma_{rr} &= [\tfrac{1}{2}(\sigma_1+\sigma_2)+\tfrac{1}{2}(\sigma_1-\sigma_2)\cos(2\alpha)]\cos^2(\theta) \\
&\quad + [\tfrac{1}{2}(\sigma_1+\sigma_2)-\tfrac{1}{2}(\sigma_1-\sigma_2)\cos(2\alpha)]\sin^2(\theta)+\tfrac{1}{2}(\sigma_1-\sigma_2)\sin(2\alpha)\sin(2\theta) \\
&= \tfrac{1}{2}(\sigma_1+\sigma_2)+\tfrac{1}{2}(\sigma_1-\sigma_2)\cos(2\alpha)[\cos^2(\theta)-\sin^2(\theta)] \\
&\quad + \tfrac{1}{2}(\sigma_1-\sigma_2)\sin(2\alpha)\sin(2\theta) \\
&= \tfrac{1}{2}(\sigma_1+\sigma_2)+\tfrac{1}{2}(\sigma_1-\sigma_2)[\cos(2\alpha)\cos(2\theta)+\sin(2\alpha)\sin(2\theta)] \\
&= \tfrac{1}{2}(\sigma_1+\sigma_2)+\tfrac{1}{2}(\sigma_1-\sigma_2)\cos(2\theta-2\alpha)
\end{aligned} \tag{A.7}$$

$$\begin{aligned}
\sigma_{r\theta} &= \tfrac{1}{2}\{[\tfrac{1}{2}(\sigma_1+\sigma_2)-\tfrac{1}{2}(\sigma_1-\sigma_2)\cos(2\alpha)] \\
&\quad - [\tfrac{1}{2}(\sigma_1+\sigma_2)+\tfrac{1}{2}(\sigma_1-\sigma_2)\cos(2\alpha)]\}\sin(2\theta)+\tfrac{1}{2}(\sigma_1-\sigma_2)\sin(2\alpha)\cos(2\theta) \\
&= -\tfrac{1}{2}(\sigma_1-\sigma_2)\cos(2\alpha)\sin(2\theta)+\tfrac{1}{2}(\sigma_1-\sigma_2)\sin(2\alpha)\cos(2\theta) \\
&= -\tfrac{1}{2}(\sigma_1-\sigma_2)[\sin(2\theta)\cos(2\alpha)-\cos(2\theta)\sin(2\alpha)] \\
&= -\tfrac{1}{2}(\sigma_1-\sigma_2)\sin(2\theta-2\alpha)
\end{aligned} \tag{A.8}$$

$$\begin{aligned}
\sigma_{\theta\theta} &= [\tfrac{1}{2}(\sigma_1+\sigma_2)+\tfrac{1}{2}(\sigma_1-\sigma_2)\cos(2\alpha)]\sin^2(\theta) \\
&\quad + [\tfrac{1}{2}(\sigma_1+\sigma_2)-\tfrac{1}{2}(\sigma_1-\sigma_2)\cos(2\alpha)]\cos^2(\theta)-\tfrac{1}{2}(\sigma_1-\sigma_2)\sin(2\alpha)\sin(2\theta) \\
&= \tfrac{1}{2}(\sigma_1+\sigma_2)-\tfrac{1}{2}(\sigma_1-\sigma_2)\cos(2\alpha)[\cos^2(\theta)-\sin^2(\theta)] \\
&\quad - \tfrac{1}{2}(\sigma_1-\sigma_2)\sin(2\alpha)\sin(2\theta) \\
&= \tfrac{1}{2}(\sigma_1+\sigma_2)-\tfrac{1}{2}(\sigma_1-\sigma_2)[\cos(2\alpha)\cos(2\theta)+\sin(2\alpha)\sin(2\theta)] \\
&= \tfrac{1}{2}(\sigma_1+\sigma_2)-\tfrac{1}{2}(\sigma_1-\sigma_2)\cos(2\theta-2\alpha)
\end{aligned} \tag{A.9}$$

$$
\begin{aligned}
\sigma_{1,2} = \tfrac{1}{2}\{&[\sigma_{rr}\cos^2(\theta) + \sigma_{\theta\theta}\sin^2(\theta) - \sigma_{r\theta}\sin(2\theta)] \\
&+ [\sigma_{rr}\sin^2(\theta) + \sigma_{\theta\theta}\cos^2(\theta) + \sigma_{r\theta}\sin(2\theta)]\} \\
\pm \tfrac{1}{2}\{&[\sigma_{rr}\cos^2(\theta) + \sigma_{\theta\theta}\sin^2(\theta) - \sigma_{r\theta}\sin(2\theta)] \\
&- [\sigma_{rr}\sin^2(\theta) + \sigma_{\theta\theta}\cos^2(\theta) + \sigma_{r\theta}\sin(2\theta)]\}\cos(2\alpha) \\
\pm [&\tfrac{1}{2}(\sigma_{rr} - \sigma_{\theta\theta})\sin(2\theta) + \sigma_{r\theta}\cos(2\theta)]\sin(2\alpha) \\
= \tfrac{1}{2}&(\sigma_{rr} + \sigma_{\theta\theta}) \pm \tfrac{1}{2}(\sigma_{rr} - \sigma_{\theta\theta})[\cos^2(\theta) - \sin^2(\theta)]\cos(2\alpha) - \sigma_{r\theta}\sin(2\theta)\cos(2\alpha) \\
&\pm \tfrac{1}{2}(\sigma_{rr} - \sigma_{\theta\theta})\sin(2\theta)\sin(2\alpha) \pm \sigma_{r\theta}\cos(2\theta)\sin(2\alpha) \\
= \tfrac{1}{2}&(\sigma_{rr} + \sigma_{\theta\theta}) \pm \tfrac{1}{2}(\sigma_{rr} - \sigma_{\theta\theta})[\cos(2\alpha)\cos(2\theta) + \sin(2\alpha)\sin(2\theta)] \\
&\mp \sigma_{r\theta}[\sin(2\theta)\cos(2\alpha) - \cos(2\theta)\sin(2\alpha)] \\
= \tfrac{1}{2}&(\sigma_{rr} + \sigma_{\theta\theta}) \pm \tfrac{1}{2}(\sigma_{rr} - \sigma_{\theta\theta})\cos(2\theta - 2\alpha) \mp \sigma_{r\theta}\sin(2\theta - 2\alpha)
\end{aligned}
\tag{A.10}
$$

A.2 Important Stress Terms and Derivatives

A.2.1 Terms Involving the Sum of Principal Stresses

Coherent Gradient Sensing (CGS) involves the sum of principal stresses, so $\sigma_1+\sigma_2$ and its derivatives must be developed in terms of Cartesian and polar coordinates. From Equations (A.3) and (A.10), the sum of principal stresses may be written as

$$\sigma_1 + \sigma_2 = \sigma_{xx} + \sigma_{yy} = \sigma_{rr} + \sigma_{\theta\theta}. \tag{A.11}$$

Given Equation (A.11), the derivatives of $\sigma_1 + \sigma_2$ with respect to r and θ may be written as

$$\frac{\partial\sigma_1 + \sigma_2}{\partial r} = \frac{\partial(\sigma_{xx} + \sigma_{yy})}{\partial r} = \frac{\partial(\sigma_{rr} + \sigma_{\theta\theta})}{\partial r}, \tag{A.12}$$

$$\frac{\partial\sigma_1 + \sigma_2}{\partial \theta} = \frac{\partial(\sigma_{xx} + \sigma_{yy})}{\partial \theta} = \frac{\partial(\sigma_{rr} + \sigma_{\theta\theta})}{\partial \theta}. \tag{A.13}$$

With Equations (A.11)–(A.13), the derivatives of $\sigma_1 + \sigma_2$ with respect to x and y are

$$\begin{aligned}\frac{\partial \sigma_1+\sigma_2}{\partial x} &= \frac{\partial r}{\partial x}\frac{\partial(\sigma_1+\sigma_2)}{\partial r} + \frac{\partial \theta}{\partial x}\frac{\partial(\sigma_1+\sigma_2)}{\partial \theta} \\ &= \cos(\theta)\frac{\partial(\sigma_1+\sigma_2)}{\partial r} - \frac{\sin(\theta)}{r}\frac{\partial(\sigma_1+\sigma_2)}{\partial \theta} \\ &= \cos(\theta)\frac{\partial(\sigma_{xx}+\sigma_{yy})}{\partial r} - \frac{\sin(\theta)}{r}\frac{\partial(\sigma_{xx}+\sigma_{yy})}{\partial \theta} \\ &= \cos(\theta)\frac{\partial(\sigma_{rr}+\sigma_{\theta\theta})}{\partial r} - \frac{\sin(\theta)}{r}\frac{\partial(\sigma_{rr}+\sigma_{\theta\theta})}{\partial \theta},\end{aligned} \tag{A.14}$$

$$\begin{aligned}\frac{\partial \sigma_1+\sigma_2}{\partial y} &= \frac{\partial r}{\partial y}\frac{\partial(\sigma_1+\sigma_2)}{\partial r} + \frac{\partial \theta}{\partial y}\frac{\partial(\sigma_1+\sigma_2)}{\partial \theta} \\ &= \sin(\theta)\frac{\partial(\sigma_1+\sigma_2)}{\partial r} + \frac{\cos(\theta)}{r}\frac{\partial(\sigma_1+\sigma_2)}{\partial \theta} \\ &= \sin(\theta)\frac{\partial(\sigma_{xx}+\sigma_{yy})}{\partial r} + \frac{\cos(\theta)}{r}\frac{\partial(\sigma_{xx}+\sigma_{yy})}{\partial \theta} \\ &= \sin(\theta)\frac{\partial(\sigma_{rr}+\sigma_{\theta\theta})}{\partial r} + \frac{\cos(\theta)}{r}\frac{\partial(\sigma_{rr}+\sigma_{\theta\theta})}{\partial \theta}.\end{aligned} \tag{A.15}$$

A.2.2 Terms Involving the Difference of Principal Stresses and Directions

Both photoelasticity and CGS for photoelastic materials involve the difference of principal stresses; additionally, CGC for photoelastic materials involve the derivatives of $\sigma_1 - \sigma_2$ and of α. These also must be written in terms of Cartesian and polar coordinates. The difference of principal stresses may be written in the following manner using Equation (A.3) and (A.10):

$$\begin{aligned}\sigma_1 - \sigma_2 &= (\sigma_{xx} - \sigma_{yy})\cos(2\alpha) + 2\sigma_{xy}\sin(2\alpha) \\ &= (\sigma_{rr} - \sigma_{\theta\theta})\cos(2\theta - 2\alpha) - 2\sigma_{r\theta}\sin(2\theta - 2\alpha).\end{aligned} \tag{A.16}$$

Taking the r and θ derivatives of $\sigma_1 - \sigma_2$ in terms of Cartesian coordinates produces equations that involve the r and θ derivatives of α, but using $\tan(2\alpha) = (2\sigma_{xy}/(\sigma_{xx} - \sigma_{yy}))$ can eliminate the

terms involving the derivatives of α.

$$\begin{aligned}\frac{\partial(\sigma_1-\sigma_2)}{\partial r} &= \frac{\partial(\sigma_{xx}-\sigma_{yy})}{\partial r}\cos(2\alpha)+2\frac{\partial\sigma_{xy}}{\partial r}\sin(2\alpha)\\ &\quad+2\frac{\partial\alpha}{\partial r}[2\sigma_{xy}\cos(2\alpha)-(\sigma_{xx}-\sigma_{yy})\sin(2\alpha)]\\ &= \frac{\partial(\sigma_{xx}-\sigma_{yy})}{\partial r}\cos(2\alpha)+2\frac{\partial\sigma_{xy}}{\partial r}\sin(2\alpha)\\ &\quad+2\frac{\partial\alpha}{\partial r}[2\sigma_{xy}\cos(2\alpha)-2\sigma_{xy}\cos(2\alpha)]\\ &= \frac{\partial(\sigma_{xx}-\sigma_{yy})}{\partial r}\cos(2\alpha)+2\frac{\partial\sigma_{xy}}{\partial r}\sin(2\alpha)\end{aligned} \tag{A.17}$$

$$\begin{aligned}\frac{\partial(\sigma_1-\sigma_2)}{\partial \theta} &= \frac{\partial(\sigma_{xx}-\sigma_{yy})}{\partial \theta}\cos(2\alpha)+2\frac{\partial\sigma_{xy}}{\partial \theta}\sin(2\alpha)\\ &\quad+2\frac{\partial\alpha}{\partial \theta}[2\sigma_{xy}\cos(2\alpha)-(\sigma_{xx}-\sigma_{yy})\sin(2\alpha)]\\ &= \frac{\partial(\sigma_{xx}-\sigma_{yy})}{\partial \theta}\cos(2\alpha)+2\frac{\partial\sigma_{xy}}{\partial \theta}\sin(2\alpha)\\ &\quad+2\frac{\partial\alpha}{\partial \theta}[2\sigma_{xy}\cos(2\alpha)-2\sigma_{xy}\cos(2\alpha)]\\ &= \frac{\partial(\sigma_{xx}-\sigma_{yy})}{\partial \theta}\cos(2\alpha)+2\frac{\partial\sigma_{xy}}{\partial \theta}\sin(2\alpha)\end{aligned} \tag{A.18}$$

Writing these derivatives in terms of polar coordinates first requires determining r and θ derivatives of $\sigma_{xx}-\sigma_{yy}$ and σ_{xy}:

$$\begin{aligned}\sigma_{xx}-\sigma_{yy} &= \sigma_{rr}(\cos^2(\theta)-\sin^2(\theta))-\sigma_{\theta\theta}(\cos^2(\theta)-\sin^2(\theta))-2\sigma_{r\theta}\sin(2\theta)\\ &= (\sigma_{rr}-\sigma_{\theta\theta})\cos(2\theta)-2\sigma_{r\theta}\sin(2\theta)\end{aligned} \tag{A.19}$$

$$\frac{\partial(\sigma_{xx}-\sigma_{yy})}{\partial r} = \frac{\partial(\sigma_{rr}-\sigma_{\theta\theta})}{\partial r}\cos(2\theta)-2\frac{\partial\sigma_{r\theta}}{\partial r}\sin(2\theta) \tag{A.20}$$

$$\frac{\partial(\sigma_{xx}-\sigma_{yy})}{\partial \theta} = \Big[\frac{\partial(\sigma_{rr}-\sigma_{\theta\theta})}{\partial \theta}-4\sigma_{r\theta}\Big]\cos(2\theta)-2\Big[\frac{\partial\sigma_{r\theta}}{\partial\theta}+(\sigma_{rr}-\sigma_{\theta\theta})\Big]\sin(2\theta). \tag{A.21}$$

With Equations (A.17), (A.18), (A.20), and (A.21), the r and θ derivatives of $\sigma_1-\sigma_2$ may be

written in terms of polar coordinates:

$$\frac{\partial(\sigma_1-\sigma_2)}{\partial r} = \frac{\partial(\sigma_{rr}-\sigma_{\theta\theta})}{\partial r}\cos(2\theta-2\alpha) - 2\frac{\partial\sigma_{r\theta}}{\partial r}\sin(2\theta-2\alpha) \tag{A.22}$$

$$\frac{\partial(\sigma_1-\sigma_2)}{\partial \theta} = \frac{\partial(\sigma_{rr}-\sigma_{\theta\theta})}{\partial \theta}\cos(2\theta-2\alpha) - 2\frac{\partial\sigma_{r\theta}}{\partial \theta}\sin(2\theta-2\alpha) - 2(\sigma_{rr}-\sigma_{\theta\theta})\sin(2\theta-2\alpha) - 4\sigma_{r\theta}\cos(2\theta-2\alpha). \tag{A.23}$$

The x and y derivatives of $\sigma_1-\sigma_2$ in terms of Cartesian and polar coordinates are easily obtained from Equations (A.17), (A.18), (A.22), and (A.23).

$$\begin{aligned}\frac{\partial(\sigma_1-\sigma_2)}{\partial x} &= \cos(\theta)\frac{\partial(\sigma_1-\sigma_2)}{\partial r} - \frac{\sin(\theta)}{r}\frac{\partial(\sigma_1-\sigma_2)}{\partial \theta} \\ &= \Big[\cos(\theta)\frac{\partial(\sigma_{xx}-\sigma_{yy})}{\partial r} - \frac{\sin(\theta)}{r}\frac{\partial(\sigma_{xx}-\sigma_{yy})}{\partial \theta}\Big]\cos(2\alpha) \\ &\quad + 2\Big[\cos(\theta)\frac{\partial\sigma_{xy}}{\partial r} - \frac{\sin(\theta)}{r}\frac{\partial\sigma_{xy}}{\partial \theta}\Big]\sin(2\alpha)\end{aligned} \tag{A.24}$$

$$\begin{aligned}\frac{\partial(\sigma_1-\sigma_2)}{\partial y} &= \sin(\theta)\frac{\partial(\sigma_1-\sigma_2)}{\partial r} + \frac{\cos(\theta)}{r}\frac{\partial(\sigma_1-\sigma_2)}{\partial \theta} \\ &= \Big[\sin(\theta)\frac{\partial(\sigma_{xx}-\sigma_{yy})}{\partial r} + \frac{\cos(\theta)}{r}\frac{\partial(\sigma_{xx}-\sigma_{yy})}{\partial \theta}\Big]\cos(2\alpha) \\ &\quad + 2\Big[\sin(\theta)\frac{\partial\sigma_{xy}}{\partial r} + \frac{\cos(\theta)}{r}\frac{\partial\sigma_{xy}}{\partial \theta}\Big]\sin(2\alpha)\end{aligned} \tag{A.25}$$

$$\begin{aligned}\frac{\partial(\sigma_1-\sigma_2)}{\partial x} &= \cos(\theta)\frac{\partial(\sigma_1-\sigma_2)}{\partial r} - \frac{\sin(\theta)}{r}\frac{\partial(\sigma_1-\sigma_2)}{\partial \theta} \\ &= \Big[\cos(\theta)\frac{\partial(\sigma_{rr}-\sigma_{\theta\theta})}{\partial r} - \frac{\sin(\theta)}{r}\Big(\frac{\partial(\sigma_{rr}-\sigma_{\theta\theta})}{\partial \theta} - 4\sigma_{r\theta}\Big)\Big]\cos(2\theta-2\alpha) \\ &\quad - 2\Big[\cos(\theta)\frac{\partial\sigma_{r\theta}}{\partial r} - \frac{\sin(\theta)}{r}\Big(\frac{\partial\sigma_{r\theta}}{\partial \theta} + (\sigma_{rr}-\sigma_{\theta\theta})\Big)\Big]\sin(2\theta-2\alpha)\end{aligned} \tag{A.26}$$

$$\begin{aligned}\frac{\partial(\sigma_1-\sigma_2)}{\partial y} &= \sin(\theta)\frac{\partial(\sigma_1-\sigma_2)}{\partial r} + \frac{\cos(\theta)}{r}\frac{\partial(\sigma_1-\sigma_2)}{\partial \theta} \\ &= \Big[\sin(\theta)\frac{\partial(\sigma_{rr}-\sigma_{\theta\theta})}{\partial r} + \frac{\cos(\theta)}{r}\Big(\frac{\partial(\sigma_{rr}-\sigma_{\theta\theta})}{\partial \theta} - 4\sigma_{r\theta}\Big)\Big]\cos(2\theta-2\alpha) \\ &\quad - 2\Big[\sin(\theta)\frac{\partial\sigma_{r\theta}}{\partial r} + \frac{\cos(\theta)}{r}\Big(\frac{\partial\sigma_{r\theta}}{\partial \theta} + (\sigma_{rr}-\sigma_{\theta\theta})\Big)\Big]\sin(2\theta-2\alpha)\end{aligned} \tag{A.27}$$

The analysis for CGS for photoelastic materials requires determining the x and y derivatives of α; this first requires the r and θ derivatives of α, which come from taking the r and θ derivatives of $\tan(2\alpha) = 2\sigma_{xy}/(\sigma_{xx} - \sigma_{yy})$:

$$\begin{aligned}
\frac{\partial}{\partial r}[\tan(2\alpha)] &= \frac{\partial}{\partial r}\Big[\frac{2\sigma_{xy}}{\sigma_{xx} - \sigma_{yy}}\Big] \\
\frac{\partial \alpha}{\partial r}\frac{2}{\cos^2(2\alpha)} &= \frac{\partial \sigma_{xy}}{\partial r}\frac{2}{\sigma_{xx} - \sigma_{yy}} - \frac{\partial(\sigma_{xx} - \sigma_{yy})}{\partial r}\frac{2\sigma_{xy}}{(\sigma_{xx} - \sigma_{yy})^2} \\
\frac{\partial \alpha}{\partial r} &= \frac{\cos^2(2\alpha)}{\sigma_{xx} - \sigma_{yy}}\Big[\frac{\partial \sigma_{xy}}{\partial r} - \frac{\tan(2\alpha)}{2}\frac{\partial(\sigma_{xx} - \sigma_{yy})}{\partial r}\Big],
\end{aligned} \tag{A.28}$$

$$\begin{aligned}
\frac{\partial}{\partial \theta}[\tan(2\alpha)] &= \frac{\partial}{\partial \theta}\Big[\frac{2\sigma_{xy}}{\sigma_{xx} - \sigma_{yy}}\Big] \\
\frac{\partial \alpha}{\partial \theta}\frac{2}{\cos^2(2\alpha)} &= \frac{\partial \sigma_{xy}}{\partial \theta}\frac{2}{\sigma_{xx} - \sigma_{yy}} - \frac{\partial(\sigma_{xx} - \sigma_{yy})}{\partial \theta}\frac{2\sigma_{xy}}{(\sigma_{xx} - \sigma_{yy})^2} \\
\frac{\partial \alpha}{\partial \theta} &= \frac{\cos^2(2\alpha)}{\sigma_{xx} - \sigma_{yy}}\Big[\frac{\partial \sigma_{xy}}{\partial \theta} - \frac{\tan(2\alpha)}{2}\frac{\partial(\sigma_{xx} - \sigma_{yy})}{\partial \theta}\Big].
\end{aligned} \tag{A.29}$$

The x and y derivatives of α may be written as

$$\begin{aligned}
\frac{\partial \alpha}{\partial x} &= \cos(\theta)\frac{\partial \alpha}{\partial r} - \frac{\sin(\theta)}{r}\frac{\partial \alpha}{\partial \theta} \\
&= \frac{\cos^2(2\alpha)}{\sigma_{xx} - \sigma_{yy}}\Big\{\cos(\theta)\Big[\frac{\partial \sigma_{xy}}{\partial r} - \frac{\tan(2\alpha)}{2}\frac{\partial(\sigma_{xx} - \sigma_{yy})}{\partial r}\Big] \\
&\qquad - \frac{\sin(\theta)}{r}\Big[\frac{\partial \sigma_{xy}}{\partial \theta} - \frac{\tan(2\alpha)}{2}\frac{\partial(\sigma_{xx} - \sigma_{yy})}{\partial \theta}\Big]\Big\},
\end{aligned} \tag{A.30}$$

$$\begin{aligned}
\frac{\partial \alpha}{\partial y} &= \sin(\theta)\frac{\partial \alpha}{\partial r} + \frac{\cos(\theta)}{r}\frac{\partial \alpha}{\partial \theta} \\
&= \frac{\cos^2(2\alpha)}{\sigma_{xx} - \sigma_{yy}}\Big\{\sin(\theta)\Big[\frac{\partial \sigma_{xy}}{\partial r} - \frac{\tan(2\alpha)}{2}\frac{\partial(\sigma_{xx} - \sigma_{yy})}{\partial r}\Big] \\
&\qquad + \frac{\cos(\theta)}{r}\Big[\frac{\partial \sigma_{xy}}{\partial \theta} - \frac{\tan(2\alpha)}{2}\frac{\partial(\sigma_{xx} - \sigma_{yy})}{\partial \theta}\Big]\Big\}.
\end{aligned} \tag{A.31}$$

Appendix B

Derivation of Analytical Solutions for Various Loading Conditions

B.1 V-Notch Stress Field Derivation

Williams (1952) presented a derivation of the stress fields of a thin plate with an "angular corner" cut out of it under uniaxial tensile load with various boundary conditions. This derivation is most commonly utilized for the derivation of the stress field of a Mode-I crack, which is a corner of angle 0^o, in a plate. Here, the derivation is applied to a thin plate with a 60^o V-shaped notch under uniaxial compression, as shown in Figure B.1. β is the angle of the material about the notch tip at the origin; therefore here $\beta = 300^o = 5\pi/3$. The V-notch is symmetric about the x-axis, and the compressive load is applied along the y-axis. The free-free boundary conditions are for the edges of the corner and not the boundaries of the plate, since the solution is for an infinite plate: $\sigma_{r\theta} = \sigma_{\theta\theta} = 0$ at $\theta = \pm\beta/2$.

The 2D stress field for this configuration may be derived using the following Airy stress potential:

$$\phi(r, \theta) = r^{\lambda+1} F(\theta), \tag{B.1}$$

where $F(\theta)$ solves the differential equation

$$\Big(\frac{d^2}{d\theta^2} + (\lambda+1)^2\Big)\Big(\frac{d^2}{d\theta^2} + (\lambda-1)^2\Big)F(\theta) = 0. \tag{B.2}$$

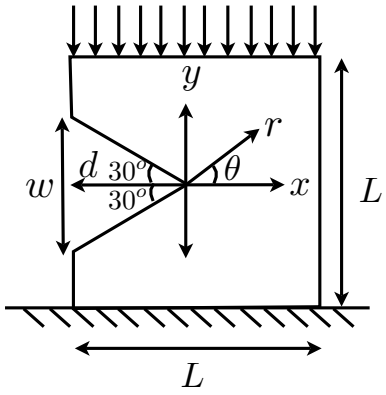

Figure B.1: Schematic of compressed plate with a side V-notch

The general solution to Equation (B.2) is

$$F(\theta) = A_1 \cos[(\lambda+1)\theta] + A_2 \sin[(\lambda+1)\theta] + A_3 \cos[(\lambda-1)\theta] + A_4 \sin[(\lambda-1)\theta]. \tag{B.3}$$

The 2D stress components are the following in terms of r, $F(\theta)$, and λ:

$$\begin{aligned}\begin{bmatrix} \sigma_{rr} & \sigma_{r\theta} \\ \sigma_{r\theta} & \sigma_{\theta\theta} \end{bmatrix} &= \begin{bmatrix} \frac{1}{r}\frac{\partial\phi}{\partial r} + \frac{1}{r^2}\frac{\partial^2\phi}{\partial\theta} & \frac{\partial^2\phi}{\partial r} \\ \frac{\partial^2\phi}{\partial r} & -\frac{\partial}{\partial r}\left(\frac{1}{r}\frac{\partial\phi}{\partial\theta}\right) \end{bmatrix} \\ &= \begin{bmatrix} r^{\lambda-1}[F''(\theta) + (\lambda+1)F(\theta)] & -\lambda r^{\lambda-1}F'(\theta) \\ -\lambda r^{\lambda-1}F'(\theta) & \lambda(\lambda+1)r^{\lambda+1}F(\theta) \end{bmatrix}. \end{aligned} \tag{B.4}$$

The $F'(\theta)$ and $F''(\theta)$ are

$$\begin{aligned} F'(\theta) = &-(\lambda+1)A_1 \sin[(\lambda+1)\theta] + (\lambda+1)A_2 \cos[(\lambda+1)\theta] \\ &-(\lambda-1)A_3 \sin[(\lambda-1)\theta] + (\lambda-1)A_4 \cos[(\lambda-1)\theta] \end{aligned} \tag{B.5}$$

$$\begin{aligned} F''(\theta) = &-(\lambda+1)^2 A_1 \cos[(\lambda+1)\theta] - (\lambda+1)^2 A_2 \sin[(\lambda+1)\theta] \\ &-(\lambda-1)^2 A_3 \cos[(\lambda-1)\theta] - (\lambda-1)^2 A_4 \sin[(\lambda-1)\theta]. \end{aligned} \tag{B.6}$$

In light of the traction-free boundary conditions at $\theta = \pm\beta/2$ and the above equations for stress,

the following equations involving λ emerge:

$$\sigma_{\theta\theta}\big|_{\theta=+\frac{\beta}{2}} = 0 = \lambda(\lambda+1)r^{\lambda-1}\{A_1\cos[(\lambda+1)\tfrac{\beta}{2}] + A_2\sin[(\lambda+1)\tfrac{\beta}{2}] + A_3\cos[(\lambda-1)\tfrac{\beta}{2}] + A_4\sin[(\lambda-1)\tfrac{\beta}{2}]\} \tag{B.7}$$

$$\sigma_{\theta\theta}\big|_{\theta=-\frac{\beta}{2}} = 0 = \lambda(\lambda+1)r^{\lambda-1}\{A_1\cos[(\lambda+1)\tfrac{\beta}{2}] - A_2\sin[(\lambda+1)\tfrac{\beta}{2}] + A_3\cos[(\lambda-1)\tfrac{\beta}{2}] - A_4\sin[(\lambda-1)\tfrac{\beta}{2}]\} \tag{B.8}$$

$$\sigma_{r\theta}\big|_{\theta=+\frac{\beta}{2}} = 0 = -\lambda r^{\lambda-1}\{-(\lambda+1)A_1\sin[(\lambda+1)\tfrac{\beta}{2}] + (\lambda+1)A_2\cos[(\lambda+1)\tfrac{\beta}{2}] - (\lambda-1)A_3\sin[(\lambda-1)\tfrac{\beta}{2}] + (\lambda-1)A_4\cos[(\lambda-1)\tfrac{\beta}{2}]\} \tag{B.9}$$

$$\sigma_{r\theta}\big|_{\theta=-\frac{\beta}{2}} = 0 = -\lambda r^{\lambda-1}\{(\lambda+1)A_1\sin[(\lambda+1)\tfrac{\beta}{2}] + (\lambda+1)A_2\cos[(\lambda+1)\tfrac{\beta}{2}] + (\lambda-1)A_3\sin[(\lambda-1)\tfrac{\beta}{2}] + (\lambda-1)A_4\cos[(\lambda-1)\tfrac{\beta}{2}]\}. \tag{B.10}$$

Constants A_1–A_4 cannot be uniquely determined solely from the four boundary conditions because Equations (B.7)–(B.10) form a homogenous system of equations; therefore the determinant of this system must go to zero. Williams (1952) determined the eigen-equation for this free-free boundary condition:

$$\sin(\lambda\beta) = \pm\lambda\frac{\sin(\beta)}{\beta}. \tag{B.11}$$

Equation (B.11) determines the values of λ as a function of β. For continuity of displacements, $\lambda > 0$. The *min Re* λ such that $\lambda > 0$ is chosen, which results in unbounded stresses near the tip of the notch. For $\beta = 5\pi/3$, this λ is $\lambda_o = 0.512221$. Therefore, the Airy stress potential is Equation (B.12) in terms of A_1 and A_2:

$$\phi(r,\theta) = r^{\lambda_o+1}\Big[A_1\Big\{\cos[(\lambda_o+1)\theta] - \frac{\cos[(\lambda_o+1)\frac{\beta}{2}]}{\cos[(\lambda_o-1)\frac{\beta}{2}]}\cos[(\lambda_o-1)\theta]\Big\} A_2\Big\{\sin[(\lambda_o+1)\theta] - \frac{\sin[(\lambda_o+1)\frac{\beta}{2}]}{\sin[(\lambda_o-1)\frac{\beta}{2}]}\sin[(\lambda_o-1)\theta]\Big\}\Big]. \tag{B.12}$$

With uniaxial extension or compression along the y axis, only the symmetric portion of the Airy

stress potential applies, as given in Equation (B.13).

$$\phi^{sym}(r,\theta) = A_1 r^{\lambda_o+1}\Big\{\cos[(\lambda_o+1)\theta] - \frac{\cos[(\lambda_o+1)\frac{\beta}{2}]}{\cos[(\lambda_o-1)\frac{\beta}{2}]}\cos[(\lambda_o-1)\theta]\Big\}. \tag{B.13}$$

With Equations (B.4) and (B.13), the 2D stresses may be written in terms of the constant A_1:

$$\sigma_{rr}(r,\theta) = \frac{A_1}{r^{1-\lambda_o}}\Big\{-\lambda_o(\lambda_o+1)\cos[(\lambda_o+1)\theta] + \lambda_o(\lambda_o-3)\frac{\cos[(\lambda_o+1)\frac{\beta}{2}]}{\cos[(\lambda_o-1)\frac{\beta}{2}]}\cos[(\lambda_o-1)\theta]\Big\} \tag{B.14}$$

$$\sigma_{\theta\theta}(r,\theta) = \frac{A_1\lambda_o(\lambda_o+1)}{r^{1-\lambda_o}}\Big\{\cos[(\lambda_o+1)\theta] - \frac{\cos[(\lambda_o+1)\frac{\beta}{2}]}{\cos[(\lambda_o-1)\frac{\beta}{2}]}\cos[(\lambda_o-1)\theta]\Big\} \tag{B.15}$$

$$\sigma_{r\theta}(r,\theta) = \frac{A_1\lambda_o}{r^{1-\lambda_o}}\Big\{(\lambda_o+1)\sin[(\lambda_o+1)\theta] - (\lambda_o-1)\frac{\cos[(\lambda_o+1)\frac{\beta}{2}]}{\cos[(\lambda_o-1)\frac{\beta}{2}]}\sin[(\lambda_o-1)\theta]\Big\}. \tag{B.16}$$

The constant A_1 is related to the applied stress in the far-field. Since the 2D stress field is in units of N/m^2, then A_1 is linearly related to applied stress, σ_{app}, and is related to the depth of the V-notch, d, to the power $1-\lambda_o$, such that

$$A_1 = C\sigma_{app}d^{1-\lambda_o}, \tag{B.17}$$

where C is a fitting constant depending on specimen geometry. With this factor, the 2D stresses become

$$\sigma_{rr}(r,\theta) = \frac{C\sigma_{app}d^{1-\lambda_o}}{(r)^{1-\lambda_o}}\Big\{-\lambda_o(\lambda_o+1)\cos[(\lambda_o+1)\theta] + \lambda_o(\lambda_o-3)\frac{\cos[(\lambda_o+1)\frac{\beta}{2}]}{\cos[(\lambda_o-1)\frac{\beta}{2}]}\cos[(\lambda_o-1)\theta]\Big\} \tag{B.18}$$

$$\sigma_{\theta\theta}(r,\theta) = \frac{C\sigma_{app}d^{1-\lambda_o}\lambda_o(\lambda_o+1)}{(r)^{1-\lambda_o}}\Big\{\cos[(\lambda_o+1)\theta] - \frac{\cos[(\lambda_o+1)\frac{\beta}{2}]}{\cos[(\lambda_o-1)\frac{\beta}{2}]}\cos[(\lambda_o-1)\theta]\Big\} \tag{B.19}$$

$$\sigma_{r\theta}(r,\theta) = \frac{C\sigma_{app}d^{1-\lambda_o}\lambda_o}{(r)^{1-\lambda_o}}\Big\{(\lambda_o+1)\sin[(\lambda_o+1)\theta] - (\lambda_o-1)\frac{\cos[(\lambda_o+1)\frac{\beta}{2}]}{\cos[(\lambda_o-1)\frac{\beta}{2}]}\sin[(\lambda_o-1)\theta]\Big\}. \tag{B.20}$$

Appendix C

Phase-Shifting Photoelasticity

Pockels developed a mathematical theory for photoelasticity in crystals known as Pockels' Phenomenological Theory (Narasimhamurty, 1981). This theory can be used to develop the well-known Stress Optic Law for photoelastic materials that are isotropic in structure and to develop stress-related equations for refractive index change in crystalline materials. The basics of this theory, based on (Narasimhamurty, 1981), are presented in this appendix, and the Stress Optic Law is derived.

A flexible and comprehensive method for analysis of a polariscope is by the use of matrices representing the action of each type of polarizing optic, i.e., using the matrix theory of photoelasticity. Theocaris and Gdoutos (1979) presented the matrices for Jones matrix algebra, which assumes that the incident light is polarized. The equations for the electric field after a polariscope result from Jones matrix algebra. The intensity of the interference pattern may then be calculated. Another, more general, method to determine the intensity of the images from a polariscope is Mueller calculus with Stokes vectors. This method does not require that the incoming light be polarized. A full treatment of Jones matrix algebra and Mueller calculus applied to the circular polariscope follows in this appendix.

By using appropriate configurations of the circular polariscope elements, different interference patterns related to the isoclinic angle and the isochromatic phase may be manipulated during analysis of the patterns to separate these two quantities of interest. This type of phase shifting is unlike the common methods that introduce a known phase shift, but capitalizes on the adaptability of the

circular polariscope to achieve different trigonometric functions of the desired phases. The entire derivation of the six-step method used in this research is provided below.

C.1 Photoelasticity of Crystals: Pockels' Phenomenological Theory

The impermeability tensor $(1/K)_{ij}$ is given by $B_{ij} = 1/n_{ij}^2$. The triaxial ellipsoid surface called the optical index ellipsoid has the formula $B_{ij}x_ix_j = 1$. The optical properties of crystals are often expressed in terms of the principal refractive indicies, by way of the refractive index ellipsoid, given by

$$\frac{x^2}{n_x^2} + \frac{y^2}{n_y^2} + \frac{z^2}{n_z^2} = 1. \tag{C.1}$$

The assumptions used in this theory are the following:

1. In a homogeneously deformed solid, the effect of deformation is only to alter the optical parameters of the optical index ellipsoid.

2. When the strain is within the elastic limits, the change of an optical parameter (polarization constant) of the solid due to deformation can be expressed as a homogeneous linear function of the nine stress components, σ_{ij}, or nine strain components, ϵ_{ij}.

C.1.1 Mathematical Formulation in Terms of the Photoelastic Constants

An undeformed crystal has an index ellipsoid of $B_{ij}^o x_i x_j = 1$. A stressed crystal has an index ellipsoid of $B_{ij}x_ix_j = 1$. Using the second assumption about linearity of the stress (strain)-impermeability tensor, then

$$B_{ij} - B_{ij}^o = -q_{ijkl}\sigma_{kl} \tag{C.2}$$

$$B_{ij} - B_{ij}^o = p_{ijkl}\epsilon_{kl}. \tag{C.3}$$

The p_{ijkl} components are called the strain-optical or elasto-optic constants. The q_{ijkl} components are called the stress-optical or piezo-optic coefficients

Assuming the ΔB_{ij}, σ_{kl}, and ϵ_{kl} second-rank tensors are symmetric, then the 81 components of the q_{ijkl} fourth-rank tensor reduce to 36 independent components ($q_{ijkl} = q_{jikl}$ and $q_{ijkl} = q_{ijlk}$), and also the 81 components of the p_{ijkl} fourth-rank tensor reduce to 36 independent components ($p_{ijkl} = p_{jikl}$ and $p_{ijkl} = p_{ijlk}$). The p_{ijkl} and q_{ijkl} tensors can be related by the elastic stiffness constants, c_{ijkl}, and compliance constants, s_{ijkl}:

$$q_{ijkl} = p_{ijmn} s_{mnkl} \tag{C.4}$$

$$p_{ijmn} = q_{ijkl} c_{klmn}. \tag{C.5}$$

The common notation uses two suffixes. The impermeability tensor B_{ij} can be written as B_i with $i = 1 - 6$ ($B_{11} = B_1$, $B_{22} = B_2$, $B_{33} = B$, $B_{23} = B_4$, $B_{31} = B_5$, and $B_{12} = B_6$). The stress and strain tensors adopt the same corresponding notation as the impermeability tensor. The photoelastic coefficient tensors, p_{ijkl} and q_{ijkl}, are written as p_{ij} and q_{ij} with $i, j = 1 - 6$. The governing photoelastic equations Equation (C.2) and Equation (C.3) become

$$B_i - B_i^o = -q_{ij} \sigma_j \tag{C.6}$$

$$B_i - B_i^o = p_{ij} \epsilon_j. \tag{C.7}$$

With this two-suffix notation, the relationships between p_{ij} and q_{ij} are related by c_{ij} and s_{ij} with $i, j = 1 - 6$:

$$p_{ij} = q_{ik} c_{kj} \tag{C.8}$$

$$q_{ij} = p_{ik} s_{kj}. \tag{C.9}$$

C.1.2 Considering Crystal Symmetry

The above mathematics applies most generally to triclinic crystals. The photoelastic coefficients can be further simplified with higher crystal symmetry. The isotropic case reduces the photoelastic tensors to two independent coefficients each:

$$p^{isotropic} = \begin{bmatrix} p_{11} & p_{12} & p_{12} & 0 & 0 & 0 \\ p_{12} & p_{11} & p_{12} & 0 & 0 & 0 \\ p_{12} & p_{12} & p_{11} & 0 & 0 & 0 \\ 0 & 0 & 0 & \frac{1}{2}(p_{11} - p_{12}) & 0 & 0 \\ 0 & 0 & 0 & 0 & \frac{1}{2}(p_{11} - p_{12}) & 0 \\ 0 & 0 & 0 & 0 & 0 & \frac{1}{2}(p_{11} - p_{12}) \end{bmatrix} \tag{C.10}$$

$$q^{isotropic} = \begin{bmatrix} q_{11} & q_{12} & q_{12} & 0 & 0 & 0 \\ q_{12} & q_{11} & q_{12} & 0 & 0 & 0 \\ q_{12} & q_{12} & q_{11} & 0 & 0 & 0 \\ 0 & 0 & 0 & (q_{11} - q_{12}) & 0 & 0 \\ 0 & 0 & 0 & 0 & (q_{11} - q_{12}) & 0 \\ 0 & 0 & 0 & 0 & 0 & (q_{11} - q_{12}) \end{bmatrix}. \tag{C.11}$$

A cubic crystal systems in group 11, (T_d, O, O_h ($4\bar{3}m$, 43, $m3m$)), reduce to three constants;

magnesium oxide (MgO) has this symmetry.

$$p^{cubic-11} = \begin{bmatrix} p_{11} & p_{12} & p_{12} & 0 & 0 & 0 \\ p_{12} & p_{11} & p_{12} & 0 & 0 & 0 \\ p_{12} & p_{12} & p_{11} & 0 & 0 & 0 \\ 0 & 0 & 0 & p_{44} & 0 & 0 \\ 0 & 0 & 0 & 0 & p_{44} & 0 \\ 0 & 0 & 0 & 0 & 0 & p_{44} \end{bmatrix} \tag{C.12}$$

$$q^{cubic-11} = \begin{bmatrix} q_{11} & q_{12} & q_{12} & 0 & 0 & 0 \\ q_{12} & q_{11} & q_{12} & 0 & 0 & 0 \\ q_{12} & q_{12} & q_{11} & 0 & 0 & 0 \\ 0 & 0 & 0 & q_{44} & 0 & 0 \\ 0 & 0 & 0 & 0 & q_{44} & 0 \\ 0 & 0 & 0 & 0 & 0 & q_{44} \end{bmatrix}. \tag{C.13}$$

C.1.3 Connection to Linearized Theory

The isotropic case greatly simplifies the photoelastic equations:

$$B_1 - B_1^o = -(q_{11}\sigma_1 + q_{12}\sigma_2 + q_{12}\sigma_3) \tag{C.14}$$

$$B_2 - B_2^o = -(q_{12}\sigma_1 + q_{11}\sigma_2 + q_{12}\sigma_3) \tag{C.15}$$

$$B_3 - B_3^o = -(q_{12}\sigma_1 + q_{12}\sigma_2 + q_{11}\sigma_3) \tag{C.16}$$

$$B_4 - B_4^o = -(q_{11} - q_{12})\sigma_4 \tag{C.17}$$

$$B_5 - B_5^o = -(q_{11} - q_{12})\sigma_5 \tag{C.18}$$

$$B_6 - B_6^o = -(q_{11} - q_{12})\sigma_6. \tag{C.19}$$

For an isotropic material, $B_1^o = B_2^o = B_3^o = (1/(n_o^2))$, where n_o is the refractive index of the unstressed material; also, $B_4^o = B_5^o = B_6^o = 0$. By manipulating Equations (C.14)–C.16), the following equations result:

$$\frac{1}{n_1^2} - \frac{1}{n_2^2} = -(q_{11} - q_{12})(\sigma_1 - \sigma_2) \tag{C.20}$$

$$\frac{1}{n_1^2} - \frac{1}{n_3^2} = -(q_{11} - q_{12})(\sigma_1 - \sigma_3) \tag{C.21}$$

$$\frac{1}{n_2^2} - \frac{1}{n_3^2} = -(q_{11} - q_{12})(\sigma_2 - \sigma_3). \tag{C.22}$$

If the quadratic refractive index term is ignored, then $B_i - B_j$ terms can be simplified. For example,

$$\begin{aligned} \frac{1}{n_1^2} - \frac{1}{n_2^2} &= \frac{n_2^2 - n_1^2}{n_1^2 n_2^2} \\ &\simeq \frac{-(n_1 - n_2)(n_1 + n_2)}{n_o^4} \\ &\simeq \frac{-(n_1 - n_2)(2n_o)}{n_o^4} \\ &\simeq \frac{-(n_1 - n_2)}{n_o^3/2}, \end{aligned} \tag{C.23}$$

assuming $n_1^2 n_2^2 \simeq n_o^4$ and $(n_1 + n_2) \simeq 2n_o$. Equations (C.20)–C.22) become the following:

$$n_1 - n_2 = \frac{n_o^3}{2}(q_{11} - q_{12})(\sigma_1 - \sigma_2) \tag{C.24}$$

$$n_1 - n_3 = \frac{n_o^3}{2}(q_{11} - q_{12})(\sigma_1 - \sigma_3) \tag{C.25}$$

$$n_2 - n_3 = \frac{n_o^3}{2}(q_{11} - q_{12})(\sigma_2 - \sigma_3) \tag{C.26}$$

The Maxwell equations for the photoelastic effect for isotropic materials are the above Equations (C.24)–C.26, given $(n_o^3/2)(q_{11} - q_{12}) = (C_1 - C_2) = C$, where C is the relative stress-optic coefficient. If the coordinate system is in the principal axes, then $\sigma_4 = \sigma_5 = \sigma_6 = 0$, and σ_1, σ_2, and σ_3 are the principal stresses.

The cubic equations with three constants result in the same relations as the isotropic case. In the plane stress case, σ_3 is zero. If the third principal axis is the optical axis, then only Equation (C.24)

needs to be considered experimentally.

C.1.4 Stress Optic Law

A photoelastic plate under stress acts as a linear retarder plate for polarized light with linear retardation δ with a fast axis at angle α relative to the x axis. The change in refractive index in the plane perpendicular to the optical axis is related to δ by the thickness of the plate h and the wavelength λ,: $n_1 - n_2 = \delta\lambda/(2\pi h)$. Therefore, the governing equation, the Stress Optic Law, may be written as the following (Kobayashi, 1993; Narasimhamurty, 1981):

$$\sigma_1 - \sigma_2 = \frac{\delta\lambda}{2\pi c_o h} = \frac{N\lambda}{c_o h}, \tag{C.27}$$

where $N = \delta/2\pi$ is the "fringe order".

C.2 Matrix Theory of Photoelasticity and Circular Polariscopes

C.2.1 Jones Matrix Algebra

A circular polariscope includes an incident collimated beam of light, followed by a linear polarizer at angle ρ to the x axis, a 1/4 wave plate with fast axis at angle ξ to the x axis, a photoelastic material, another 1/4 wave plate with fast axis at angle ϕ to the x axis, and a second linear polarizer at angle ζ to the x axis, sometimes called the analyzer. Figure C.1 shows a schematic of the polariscope. Assuming that the collimated laser beam is polarized, then Jones matrix algebra may be used to analyze the electric field components incident to the sample (Theocaris and Gdoutos, 1979). Note: Theocaris and Gdoutos (1979) employs reference axes such that the x and y are perpendicular to the incident beam relative to the *front* of the optics. The reference axes x and y used in this research are perpendicular to the light beam, which is along the $+z$ axis, on the *back* of the optics, as shown

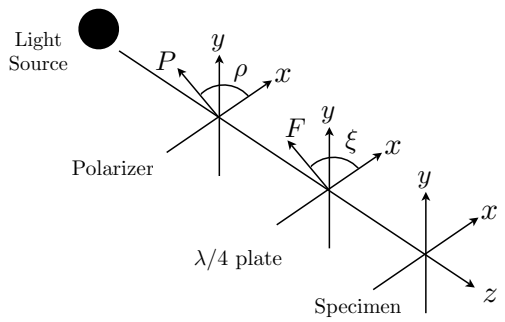

Figure C.1: Polarization optics before the transparent sample

in Figure C.1. The electric field prior to the polarizer is given in vector form by Equation (C.28):

$$\boldsymbol{E} = \begin{bmatrix} E_{ox} exp[j(kz - \omega t + \varphi_x)] \\ \\ E_{oy} exp[j(kz - \omega t + \varphi_y)] \end{bmatrix}. \tag{C.28}$$

The Jones vector, $\boldsymbol{a}$, represents the time-averaged x and y spatial amplitude and phase components of the electric field, a_x and a_y. Thus the Jones vector of the collimated light in Equation (C.28) is

$$\boldsymbol{a}^{collimated} = \begin{bmatrix} a_x \\ \\ a_y \end{bmatrix} = \begin{bmatrix} E_{ox} exp[j(kz + \varphi_x)] \\ \\ E_{oy} exp[j(kz + \varphi_y)] \end{bmatrix}. \tag{C.29}$$

After passing through a polarization optic, the electric field obviously changes, represented by the multiplication of the Jones matrix of the the polarization optic and the Jones vector of the incident electric field. Therefore, Jones matrix algebra is a compact way of determining the changes in an initially linearly polarized electric field due to polarization optics. The Jones matrices for a linear polarizer at angle ρ to the x axis and for a 1/4 wave plate with fast axis at angle ξ to the x

axis are as follows:

$$\mathbf{P}_{\rho} = \begin{bmatrix} \cos^2(\rho) & -cos(\rho)sin(\rho) \\ -cos(\rho)sin(\rho) & \sin^2(\rho) \end{bmatrix} \tag{C.30}$$

$$\mathbf{Q}_{\xi} = \begin{bmatrix} j\cos^2(\xi) + \sin^2(\xi) & (1-j)cos(\xi)sin(\xi) \\ (1-j)cos(\xi)sin(\xi) & j\sin^2(\xi) + \cos^2(\xi) \end{bmatrix}. \tag{C.31}$$

Generally, the electric field incident to the sample in Figure C.1 is given by Equation (C.32):

$$\boldsymbol{a}^{incident} = \mathbf{Q}_{\xi}\mathbf{P}_{\rho}\boldsymbol{a}^{\mathbf{collimated}}. \tag{C.32}$$

For example, if $\rho = \pi/2$ and $\xi = 3\pi/4$, then the electric field components have the same constant $A_o = \sqrt{2}E_{oy}/2$, as shown in Equation (C.33):

$$\begin{aligned} \boldsymbol{a}^{incident} = \mathbf{Q}_{\frac{3\pi}{4}}\mathbf{P}_{\frac{\pi}{2}}\boldsymbol{a}^{collimated} &= \frac{\sqrt{2}E_{oy}exp[j(kz+\varphi_y)]}{2}\begin{bmatrix} exp[j\frac{3\pi}{4}] \\ exp[j\frac{\pi}{4}] \end{bmatrix} \\ &= \begin{bmatrix} A_o exp[j(kz+\phi_x)] \\ A_o exp[j(kz+\phi_y)] \end{bmatrix}. \end{aligned} \tag{C.33}$$

A photoelastic material is modeled in terms of polarization optics as a linear retardation plate with retardation δ (the isochromatic phase) with fast axis at angle α (the isoclinic angle) to the x axis. The Jones matrix for such a linear retardation plate is as follows:

$$\mathbf{R}_{\delta,\alpha} = \begin{bmatrix} e^{j\delta}\cos^2(\alpha) + \sin^2(\alpha) & (1-e^{j\delta})cos(\alpha)sin(\alpha) \\ (1-e^{j\delta})cos(\alpha)sin(\alpha) & e^{j\delta}\sin^2(\alpha) + \cos^2(\alpha) \end{bmatrix}. \tag{C.34}$$

The general full expression for the electric field after a circular polariscope with all five elements is

as follows:

$$\boldsymbol{E}^{out} = \mathbf{P}_{\zeta}\mathbf{Q}_{\phi}\mathbf{R}_{\delta,\alpha}\mathbf{Q}_{\xi}\mathbf{P}_{\rho}\boldsymbol{E}. \tag{C.35}$$

The intensity of the resulting image is a result of taking the dot product of the final electric field with its complex conjugate:

$$I^{image} = \boldsymbol{E}^{out} \cdot \tilde{\boldsymbol{E}}^{out} = E_x^{out}\tilde{E}_x^{out} + E_y^{out}\tilde{E}_y^{out}. \tag{C.36}$$

If $\rho = \pi/2$ and $\xi = 3\pi/4$, then the intensity of the image reduces to the following:

$$I^{image} = 2E_{oy}^2\{1 + \cos(\delta)\sin[2(\zeta - \phi)] - \sin(\delta)\cos[2(\zeta - \phi)]\sin[2(\alpha - \phi)]\}. \tag{C.37}$$

C.2.2 Mueller Calculus with Stokes Vectors

A Stokes vector, denoted $\boldsymbol{S}$ is another representation of the polarization of the electric field similar to the Jones vector except the Stokes vector has four time-averaged parameters, as shown in Equation (C.38), where <> represents time averaging. The first Stokes parameter, s_o, is the intensity of the electric field, making it a convenient parameter to find the intensity of an image.

$$\boldsymbol{S} = \begin{bmatrix} s_o \\ s_1 \\ s_2 \\ s_3 \end{bmatrix} = \begin{bmatrix} < a_x\tilde{a}_x + a_y\tilde{a}_y > \\ < a_x\tilde{a}_x - a_y\tilde{a}_y > \\ < 2\Re\{a_x\tilde{a}_y\} > \\ < 2\Im\{a_x\tilde{a}_y\} > \end{bmatrix}. \tag{C.38}$$

Mueller matrices describe how the polarization changes after the light passes through a polarization optic, where the parameters of these matrices modify the Stokes vector representation of light polarization. The Mueller matrices, given the coordinate convention in Figure C.1, for a linear polarizer

at angle ρ to the x axis and for a 1/4 wave plate with fast axis at angle ξ to the x axis are as follows:

$$\mathbf{P}_{\rho}^{\mathbf{M}} = \begin{bmatrix} 1 & \cos(2\rho) & -\sin(2\rho) & 0 \\ \cos(2\rho) & \cos^2(2\rho) & -\sin(2\rho)\cos(2\rho) & 0 \\ -\sin(2\rho) & -\sin(2\rho)\cos(2\rho) & \sin^2(2\rho) & 0 \\ 0 & 0 & 0 & 0 \end{bmatrix} \tag{C.39}$$

$$\mathbf{Q}_{\xi}^{\mathbf{M}} = \begin{bmatrix} 1 & 0 & 0 & 0 \\ 0 & \cos^2(2\xi) & -\sin(2\xi)\cos(2\xi) & \sin(2\xi) \\ 0 & -\sin(2\xi)\cos(2\xi) & \sin^2(2\xi) & \cos(2\xi) \\ 0 & -\sin(2\xi) & -\cos(2\xi) & 0 \end{bmatrix}. \tag{C.40}$$

The Mueller matrix of a linear retarder with retardation δ and fast axis α, the model for a photoelastic material, is

$$\mathbf{R}_{\delta,\alpha}^{\mathbf{M}} = \begin{bmatrix} 1 & 0 & 0 & 0 \\ 0 & \cos^2(2\alpha) + \sin^2(2\alpha)\cos(\delta) & -\sin(2\alpha)\cos(2\alpha)(1-\cos(\delta)) & \sin(2\alpha)\sin(\delta) \\ 0 & -\sin(2\alpha)\cos(2\alpha)(1-\cos(\delta)) & \sin^2(2\alpha) + \cos^2(2\alpha)\cos(\delta) & \cos(2\alpha)\sin(\delta) \\ 0 & -\sin(2\alpha)\sin(\delta) & -\cos(2\alpha)\sin(\delta) & \cos(\delta) \end{bmatrix}. \tag{C.41}$$

The Stokes vector of a general circular polariscope, with two polarizers, two 1/4 wave plates, and a photoelastic material, is the multiplication of the incident Stokes vector and the Mueller matrices

of all the elements. The Stokes vector of the incident electric field is

$$\boldsymbol{S}^{incident} = \begin{bmatrix} E_{ox}^2 + E_{oy}^2 \\ E_{ox}^2 - E_{oy}^2 \\ 2E_{ox}E_{oy}\cos(\varphi_x - \varphi_y) \\ 2E_{ox}E_{oy}\sin(\varphi_x - \varphi_y) \end{bmatrix}. \tag{C.42}$$

The general form of the Stokes vector for a circular polariscope is

$$\boldsymbol{S}^{out} = \mathbf{P}_{\zeta}^{\mathbf{M}}\mathbf{Q}_{\phi}^{\mathbf{M}}\mathbf{R}_{\delta,\alpha}^{\mathbf{M}}\mathbf{Q}_{\xi}^{\mathbf{M}}\mathbf{P}_{\rho}^{\mathbf{M}}\boldsymbol{S}^{\mathbf{incident}}. \tag{C.43}$$

Given a circular polariscope with the first polarizer at angle $\rho = \pi/2$, the first 1/4 wave plate at angle $\xi = 3\pi/4$, from Equation (C.43), the first Stokes parameter, the intensity of the electric field, may be reduced to

$$I_{image} = s_o^{out} = 2E_{oy}^2\{1 + \cos(\delta)\sin[2(\zeta - \phi)] - \sin(\delta)\cos[2(\zeta - \phi)]\sin[2(\alpha - \phi)]\}, \tag{C.44}$$

which is the same as the intensity determined by Jones matrix algebra in Equation (C.37).

C.3 Six-Step Phase Shifting

With the flexibility of the polariscope optics, many different combinations of intensities involving the isoclinic angle and isochromatic phase are possible. Choosing a certain set of these intensities allows for the separation of these two phases. The set of six images chosen for this research are given in Table C.1, where the first two elements do not change angle ($\rho = \pi/2$ and $\xi = 3\pi/4$) and the second 1/4 wave plate and second polarizer are at angles ϕ and ζ, respectively. The intensities for these images come from Equation (C.44).

Image	ϕ	ζ
$I_1 = 2E_{oy}(1 + \cos(\delta))$	$\pi/2$	$3\pi/4$
$I_2 = 2E_{oy}(1 - \cos(\delta))$	$\pi/2$	$\pi/4$
$I_3 = 2E_{oy}(1 - \sin(\delta)\sin(2\theta))$	π	π
$I_4 = 2E_{oy}(1 + \sin(\delta)\cos(2\theta))$	$\pi/4$	$\pi/4$
$I_5 = 2E_{oy}(1 + \sin(\delta)\sin(2\theta))$	$\pi/2$	$\pi/2$
$I_6 = 2E_{oy}(1 - \sin(\delta)\cos(2\theta))$	$3\pi/4$	$3\pi/4$

Table C.1: Photoelasticity phase shifting: Angles refer to fast axis of optics

Bibliography

Anderson, T. L., 2005. *Fracture Mechanics: Fundamentals and Applications*. CRC Press, 3rd edition.

Ashokan, K. and Ramesh, K., 2006. A novel approach for ambiguity removal in isochromatic phasemap in digital photoelasticity. *Meas. Sci. Tech.*, 17:2891–2896.

Azhdari, A. and Nemat-Nasser, S., 1996. Energy release rate and crack kinking in anisotropic brittle solids. *J. Mech. Phys. Solids*, 44(6):929–951.

Azhdari, A. and Nemat-Nasser, S., 1998. Experimental and computational study of fracturing in an anisotropic brittle solid. *Mech. Mater.*, 28:247–262.

Azhdari, A., Nemat-Nasser, S., and Rome, J., 1998. Experimental observations and computational modeling of fracturing in an anisotropic brittle crystal (sapphire). *Int. J. Fracture*, 94:251–266.

Baldi, A., Bertolino, F., and Ginesu, F., 2002. On the performance of some unwrapping algorithms. *Opt. Laser Eng.*, 37:313–330.

Barone, S. and Patterson, E. A., 1996. Full-field separation of principal stresses by combined thermo- and photoelasticity. *Exp. Mech.*, 36(4):318–324.

Barone, S. and Patterson, E. A., 1998. Polymer coating as a strain witness in thermoelasticity. *J. Strain Anal. Eng.*, 33(3):223–232.

Berghaus, D., 1991. Combining photoelasticity and finite-element methods for stress analysis using least squares. *Exp. Mech.*, 31(1):36–41.

Bradley, W. B. and Kobayashi, A. S., 1971. Fracture dynamics—a photoelastic investigation. *Engr. Fracture Mech.*, 3(3):317–332.

Bruck, H. A. and Rosakis, A. J., 1992. On the sensitivity of coherent gradient sensing: part I—a theoretical investigation of accuracy in fracture mechanics applications. *Opt. Laser Eng.*, 17:83–101.

Bruck, H. A. and Rosakis, A. J., 1993. On the sensitivity of coherent gradient sensing: part II—an experimental investigation of accuracy in fracture mechanics applications. *Opt. Laser Eng.*, 18:25–51.

Coker, E. G. and Filon, L. N. G., 1993. *A Treatise on Photo-elasticity*. Cambridge Univeristy Press.

Cotterell, B. and Rice, J. R., 1980. Slightly curved or kinked cracks. *Int. J. Fracture*, 16(2):155–169.

Dally, J. W., 1979. Dynamic photo-elastic studies of fracture. *Exp. Mech.*, 19(10):349–361.

Ekman, M. J. and Nurse, A. D., 1998. Completely automated determination of two-dimensional photoelastic parameters using load stepping. *Opt. Eng.*, 37(6):1845–1851.

Frocht, M. M., 1941. *Photoelasticity*, volume 1. John Wiley and Sons.

Ghiglia, D. C. and Romero, L. A., 1994. Robust two-dimensional weighted and unweighted phase unwrapping that uses fast transforms and iterative methods. *J. Opt. Soc. Am. A*, 11(1):107–117.

Goldstein, R. V. and Salganik, R. L., 1974. Brittle-fracture of solids with arbitrary cracks. *Int. J. Fracture*, 10(4):507–523.

Greene, R. J., Clarke, A. B., Turner, S., and Patterson, E. A., 2007. Some applications of combined thermoelastic-photoelastic stress analysis. *J. Strain Anal. Eng.*, 42:173–182.

Haake, S. J., Patterson, E. A., and Wang, Z. F., 1996. 2D and 3D separation of stresses using automated photoelasticity. *Exp. Mech.*, 36(3):269–276.

Hecht, E., 2002. *Optics*. Pearson Education, Inc., 4th edition.

Hodgdon, J. and Sethna, J. P., 1993. Derivation of a general 3-dimensional crack-proparation law—a generalization of the principle of local symmetry. *Phys. Rev. B*, 47(9):4831–4840.

Huang, Y. M., Mohsen, H. H. A., and Rowlands, R. E., 1990a. Determination of individual stresses thermoelastically. *Exp. Mech.*, 30(1):88–94.

Huang, Y. M., Rowlands, R. E., and Lesniak, J. R., 1990b. Simultaneous stress separation, smoothing of measured thermoelastic isopachic information and enhanced boundary data. *Exp. Mech.*, 30(4):398–403.

Irwin, G. R., Dally, J. W., Kobayashi, T., Fourney, W. L., Etheridge, M. J., and Rossmanith, H. P., 1979. Determination of the A-K relationship for birefringent polymers. *Exp. Mech.*, 19(4):121–128.

Jona, F. and Shirane, G., 1993. *Ferroelectric Crystals*. Dover Publications, Inc.

Kobayashi, A. S., editor, 1993. *Handbook of Experimental Mechanics*. Wiley.

Kramer, S. L. B., Mello, M., Ravichandran, G., and Bhattacharya, K., 2009a. Phase shifting full-field interferometric methods for determination of in-plane tensorial stress. *Exp. Mech.*, 49(2):303–315.

Kramer, S. L. B., Ravichandran, G., and Bhattacharya, K., 2009b. Transmission wavefront shearing interferometry for photoelastic materials. *Appl. Opt.*, 48(13):2450–2460.

Krishnaswamy, S., 2000. *Photomechanics*, volume 77 of *Topics in Applied Physics*, chapter Techniques for Non-Birefringnet Objects: Coherent Shearing Interferometry and Caustics, pages 295–321. Springer-Verlag Berlin Heidelberg.

Krishnaswamy, S., Rosakis, A. J., and Ravichandran, G., 1991. On the extent of dominance of asymptotic elastodynamic crack-tip fields, part ii: A numerical investigation of three-dimensional and transient effects. *J. Appl. Mech.*, 58(1):95–103.

Lee, H., Rosakis, A. J., and Freund, L. B., 2001. Full-field optical measurement of curvatures in unltra-thin-film-substrate systems in the range of geometrically nonlinear deformations. *J. Appl. Phys.*, 89(11):6116–6129.

Liu, C., Rosakis, A. J., Ellis, R. W., and Stout, M. G., 1998. A study of the fracture behavior of unidirectional fiber-reinforces composites using coherent gradient sensing (CGS) interferometry. *Int. J. Fracture*, 90:355–382.

Mason, J. J., Lambros, J., and Rosakis, A. J., 1992. On the use of coherent gradient sensing in dynamic mixed-mode fracture mechancis experiments. *J. Mech. Phys. Solids*, 40(3):641–661.

Murty, M. V. R., 1964. Use of single plane parallel plate as lateral shearing interferometer with visible gas laser source. *Appl. Opt.*, 3(4):531.

Narasimhamurty, T. S., 1981. *Photoelastic and Electro-optic Properties of Crystals*. Plenum Press.

Papdopoulos, G. A., 1993. *Fracture Mechanics: The Experimental Method of Caustics and the Det. Criterion of Fracture*. Springer-Verlag.

Park, T. S., Suresh, S., Rosakis, A. J., and Ryu, J., 2003. Measurement of full-field curvatue and geometrical instability of thin film-substrate systems through CGS interferometry. *J. Mech. Phys. Solids*, 51:2191–2211.

Patterson, E. A., Ji, W., and Wang, Z. F., 1997. On image analysis for birefringence measurements in photoelasticity. *Opt. Laser Eng.*, 28:17–36.

Patterson, E. A. and Wang, Z. F., 1998. Simultaneous observation of phase-stepped images for automated photoelasticity. *J. Strain Anal. Eng.*, 33(1):1–15.

Ramesh, K., 2009. Photelasticity. In W. Sharpe, editor, *Springer Handbook of Experimental Solid Mechanics*. Springer-Verlag.

Ramesh, K. and Tamrakar, D. K., 2000. Improved determination of retardation in digital photoelasticity by load stepping. *Opt. Laser Eng.*, 33(6):387–400.

RaviChandar, K., 1982. An experimental investigation into the mechanics of dynamic fracture. Ph.D. thesis, California Institute of Technology.

Rosakis, A. J., 1993. *Experimental Techniques in Fracture*, chapter Two Optical Techniques Sensitive to Gradients of Optical Path Difference: The Method of Caustics and the Coherent Gradient Sensor (CGS), pages 327–425. Society of Experimental Mechanics.

Rosakis, A. J., Krishnaswamy, S., and Tippur, H. V., 1990. On the application of the optical methods of caustics to the investigation of transient elastodynamic crack problems: Limitations of the clasical interpretation. *Opt. Laser Eng.*, 13:183–210.

Sakagami, T., Kubo, S., Fujinami, Y., and Kojima, Y., 2004. Experimental stress separation technique using thermoelasticity and photoelasticity and its applciation to fracture mechanics. *JSME Int. J. A*, 17(3):298–304.

Sanford, R. J. and Dally, J. W., 1979. A general method for determining mixed-mode stress intensity factors from isochromatic fringe patterns. *Engr. Fracture Mech.*, 11:621–633.

Shimizu, K., Suetsugu, M., Nakamura, T., and Takahashi, S., 1998. Evaluation of concentrated load by caustics and its application in the measurement of optical constant. *JSME Int. J.*, 41(1):134–141.

Siegmann, P., Backman, D., and Patterson, E. A., 2005. A robust approach to demodulating and unwrapping phase-stepped photoelastic data. *Exp. Mech.*, 45(3):278–289.

Smith, C. W. and Olaosebikan, O., 1984. Use of mixed-mode stress-intensity algorithms for photoelastic data. *Exp. Mech.*, 24(4):300–207.

Smith, D. G. and Smith, C. W., 1972. Photoelastic determination of mixed mode stress intensity factors. *Engr. Fracture Mech.*, 4:357–366.

Theocaris, P. S. and Gdoutos, E. E., 1979. *Matrix Theory of Photoelasticity.* Springer-Verlag.

Tippur, H. V., Krishnaswamy, S., and Rosakis, A. J., 1991a. A coherent gradient sensor for crack tip deformation measurements: analysis and experimental results. *Int. J. Fracture*, 48:193–204.

Tippur, H. V., Krishnaswamy, S., and Rosakis, A. J., 1991b. Optical mapping of crack tip deformations using the methods of trasmission and reflection coherent gradient sensing: a study of crack tip K-dominance. *Int. J. Fracture*, 52(91-117).

Williams, M. L., 1952. Stress singularities resulting from various boundary conditions in angular corners of plates in extension. *J. Appl. Mech.*, pages 526–528.

Yariv, A. and Yeh, P., 2007. *Photonics: Optical Electronics in Modern Communications*. Oxford University Press, 6th edition.

Yoneyama, S., Morimoto, Y., and Kawamura, M., 2005. Two-dimensional stress separation using phase-stepping interferometric photoelasticity. *Meas. Sci. Tech.*, 16:1329–1334.